Activation of intestinal endogenous retroviruses by alcohol exacerbates liver disease

Noemí Cabré[1#], Marcos F. Fondevila[1#], Wenchao Wei[1], Tomoo Yamazaki[1,2], Fernanda Raya Tonetti[1], Alvaro Eguileor[1], Ricard Garcia-Carbonell[3], Abraham S. Meijnikman[1], Yukiko Miyamoto[1], Susan Mayo[1], Yanhan Wang[1], Xinlian Zhang[4], Thorsten Trimbuch[5], Seija Lehnardt[6], Lars Eckmann[1], Derrick E. Fouts[7], Cristina Llorente[1], Hidekazu Tsukamoto[8,9], Peter Stärkel[10] and Bernd Schnabl[1,11]

[1]Department of Medicine, University of California San Diego, La Jolla, CA, USA

[2]Department of Medicine, Division of Gastroenterology and Hepatology, Shinshu University School of Medicine, Matsumoto, Japan

[3]Department of Molecular and Cellular Biology, The Scripps Research Institute, La Jolla, CA, USA

[4]Division of Biostatistics and Bioinformatics, Herbert Wertheim School of Public Health and Human Longevity Science, University of California San Diego, La Jolla, CA, USA

[5]Institute of Neurophysiology, Charité Viral Core Facility, Charité – Universitätsmedizin Berlin, corporate member of Freie Universität Berlin, Humboldt-Universität zu Berlin, and Berlin Institute of Health, Berlin, Germany

[6]Institute of Cell Biology and Neurobiology, Charité–Universitätsmedizin Berlin, corporate member of Freie Universität Berlin, Humboldt-Universität zu Berlin, and Berlin Institute of Health (BIH), Berlin, Germany

[7]J. Craig Venter Institute, Rockville, MD, USA

[8]Department of Pathology, Keck School of Medicine of the University of Southern California, Los Angeles, CA, USA

[9]Department of Veterans Affairs Greater Los Angeles Healthcare System, Los Angeles, CA, USA

[10]Department of Hepatology and Gastroenterology, St. Luc University Hospital, Catholic University of Louvain, Brussels, Belgium

[11]Department of Medicine, VA San Diego Healthcare System, San Diego, CA, USA

[#]equal contribution

Correspondence: Bernd Schnabl, M.D., Department of Medicine, University of California San Diego, MC0063, 9500 Gilman Drive, La Jolla, CA 92093, Phone 858-822-5311, Fax 858-246-1788, Email beschnabl@ucsd.edu

Keywords: Alcoholic liver disease, microbiome, microbiota, Gut-liver axis

Abbreviations: Adh1, alcohol dehydrogenase 1; ALT, alanine aminotransferase; ANOVA, analysis of variance; AUD, alcohol use disorder; AUC, area under the curve; BMI, body mass index; CFU, colony forming unit; Ccl, C-C motif chemokine ligand; Cxcl, C-X-C motif chemokine ligand; Cyp2e1, cytochrome P450, family 2, subfamily e, polypeptide 1; DMEM, Dulbecco's modified Eagle medium; *E. coli*, *Escherichia coli*; EC, emtricitabine; ERV(s), endogenous retrovirus(es); HERV(s), human endogenous retrovirus(es); LPS; lipopolysaccharide; Mlkl, mixed lineage kinase domain-like

pseudokinase; PCR, polymerase chain reaction; RT, reverse transcriptase; TDF, tenofovir disoproxil fumarate; Zbp1, Z-DNA binding protein 1, *Zbp1*$^{\Delta IEC}$, intestinal epithelial cell specific deletion of *Zbp1*, *Zbp1*$^{\Delta KC}$, Kupffer cell specific deletion of *Zbp1*; *Zbp1*$^{\Delta Hep}$, hepatocyte specific deletion of *Zbp1*

This study was presented at the 2023 Liver Meeting of the American Association for the Study of Liver Disease (AASLD).

Abstract

Alcohol-associated liver disease represents a significant global health challenge, with gut microbial dysbiosis and bacterial translocation playing a critical role in its pathogenesis. Patients with alcohol-associated hepatitis had increased fecal abundance of mammalian viruses including retroviruses. This study investigated the role of endogenous retroviruses (ERVs) in the development of alcohol-associated liver disease. Transcriptomic analysis of duodenal and liver biopsies revealed increased expression of several human ERVs, including *HERV-K* and *HERV-H*, in patients with alcohol-associated liver disease compared with controls. Chronic-binge ethanol feeding markedly induced ERV abundance in intestinal epithelial cells, but not the liver of mice. Ethanol increased ERV expression and activated the Z-DNA binding protein 1 (Zbp1)–mixed lineage kinase domain-like pseudokinase (Mlkl) signaling pathways to induce necroptosis in intestinal epithelial cells. Antiretroviral treatment reduced ethanol-induced intestinal ERV expression, stabilized the gut barrier, and decreased liver disease in microbiota-humanized mice. Furthermore, mice with an intestine-specific deletion of *Zbp1* were protected against bacterial translocation and ethanol-induced steatohepatitis. These findings indicate that ethanol exploits this pathway by inducing ERVs and promoting innate immune responses, which results in the death of intestinal epithelial cells, gut barrier dysfunction and liver disease. Targeting the ERV-Zbp1 pathway may offer new therapies for patients with alcohol-associated liver disease.

Introduction

Alcohol-associated liver disease poses a significant global public health challenge, arising from prolonged and harmful alcohol consumption (1, 2). Chronic harmful alcohol consumption results in hepatic steatosis and can progress to hepatitis, fibrosis and cirrhosis. The gut-liver axis plays an important role in the pathogenesis of alcohol-associated liver disease (3). Alcohol consumption is associated with intestinal dysbiosis and gut barrier dysfunction. Microbial-associated molecular patterns (MAMPs) can translocate from the gut to the liver thereby contributing to liver inflammation and disease progression (4). Viable bacteria can also cross the gut barrier by mechanisms that are incompletely understood and contribute to alcohol-associated liver disease (5).

Our previous study revealed an increased abundance of mammalian viruses, including retroviruses, in the fecal virome of patients with alcohol-associated hepatitis (6). Despite this discovery, the specific role of the gut virome, particularly endogenous retroviruses (ERVs), in the development of alcohol-associated liver disease remains unknown. ERVs are ancient remnants of retroviral infections integrated into vertebrate genomes, including humans (7). Many human ERVs (HERVs) such as HERV-H and HERV-P (both gammaretrovirus-like) integrated into the genome over 30 million years ago, while some HERVs such as HERV-K (betaretrovirus-like) entered the genome more recently (8-10). ERV genomes typically contain three main genes—*gag* (coding for the viral capsid), *pol* (encoding reverse transcriptase and integrase), and *env* (responsible for envelope proteins)—along with flanking long terminal repeats (LTRs), though in most cases these sequences are non-functional, and no intact viral particles are produced (7). Originating

from retroviruses infecting germ cells, ERVs are mostly located in the heterochromatin, have undergone silencing through DNA methylation mechanisms, and have lost their coding capacity (11). Recently, ERVs have been discovered as regulatory RNAs contributing to cellular homeostasis in a healthy state (12). Under certain circumstances, ERVs are transcribed and form double-stranded RNA (13). ERVs are sensed by the innate immune system and can contribute to disease, such as cancer, infection, or autoimmune disease (14-16). For example, high-fat diet primed keratinocytes increase ERV expression and promote skin inflammation in response to commensal colonization, which is alleviated by antiretroviral therapy (16).

Z-DNA binding protein 1 (Zbp1) is a sensor for aberrant nucleic acids—such as non-coding RNA, misfolded RNA/DNA structures, or viral nucleic acids, including those derived from viral infections such as influenza A virus and cytomegalovirus (17). Zbp1 detects Z-RNA, a left-handed helical form of RNA. This structure can emerge under conditions of physiological stress or during viral infections. During influenza A virus infection, Zbp1 binds to viral Z-RNA, initiates receptor-interacting serine/threonine-protein kinase 3 (Ripk3)-mediated activation, and triggers mixed lineage kinase domain-like pseudokinase (Mlkl)-dependent necroptosis (18). Necroptosis is therefore viewed as a part of the innate host defense to eliminate virus-infected cells (18, 19). Similarly, double-stranded RNA derived from ERVs triggers Zbp1 activation and activates Ripk3-dependent necroptosis (20). Patients with inflammatory bowel disease (IBD) and reactivation of HERVs due to a dysfunctional upstream repressor SETDB1, activate ZBP1, and the

125 necroptosis pathway in intestinal stem cells, which leads to epithelial barrier damage and
126 inflammation in the intestine (21).
127
128 In this study, we examined the role of ERVs and the involvement of Zbp1 in mediating the
129 impact of ERVs on the progression of alcohol-associated liver disease.
130
131

Results

Patients with alcohol use disorder and liver disease have increased *HERV* expression in the duodenum and liver

To determine whether patients with alcohol use disorder and liver disease have increased HERV expression, we analyzed duodenal biopsies from subjects without alcohol use disorder or alcohol-associated liver disease (controls, n=16) and patients with alcohol use disorder (n=44) (**Supplementary Table 1**). Compared with controls, patients with alcohol use disorder showed a significant upregulation of *HERV-K env* and *HERV-K pol* genes (**Figure 1a**). Patients with progressive liver disease (steatohepatitis or steatofibrosis) had significantly higher expression of *HERV-K env* compared to those with non-progressive disease (simple steatosis) or controls (**Supplemental Figure 1a**). Furthermore, patients with advanced liver fibrosis (F2-F4) had increased *HERV-K env*, *HERV-K pol* and *HERV-H env* expression in the duodenum as compared with controls and patients with no or mild liver disease (**Figure 1b; Supplemental Figure 1b**). We also measured HERV expression in liver biopsies from controls (n=5) and patients with alcohol use disorder (n=27) (**Supplementary Table 2**). Patients with alcohol use disorder showed significant hepatic upregulation of *HERV-K env*, *HERV-K pol* and *HERV-H env* genes (**Figure 1c**).

To investigate the potential role of ethanol in modulating HERV expression, human intestinal organoids from four independent donors were incubated with ethanol (50 mM) (**Figure 1d**). Exposure to ethanol for 24 hours resulted in upregulation of *HERV-K env*, *HERV-K pol,* and *HERV-H env* expression (**Figure 1e**) and increased cytotoxicity, as determined by lactate dehydrogenase (LDH) release compared with vehicle-treated

organoids (**Figure 1f**). These findings indicate that ethanol alone can directly induce HERV expression in intestinal epithelial cells.

Ethanol-induced ERV expression activates Zbp1 and induces Mlkl-mediated necroptosis in intestinal epithelial cells

To determine whether mice, which also carry endogenous retroviruses (22), can serve as a model to better understand the role of ERVs in the pathogenesis of alcohol-related intestinal disease, we employed three different ethanol-induced liver disease models: 1) Chronic-binge ethanol feeding (23, 24) in microbiota humanized mice. Colonization of germ-free mice with feces from patients with alcohol-associated hepatitis is known to exacerbate ethanol-induced liver disease, compared with feces from conventional mice (24) (**Figure 2a; Supplemental Figure 2a**); 2) Chronic-binge ethanol feeding in conventional mice (23) (**Supplemental Figure 2d**); 3) Intragastric hybrid feeding model of ethanol, which combines ethanol and western diet feeding (25) (**Supplemental Figure 2g**). Expression of the murine betaretrovirus mouse mammary tumor virus (MMTV) transcripts *env* and *gag* was induced in all three murine models along the small and large intestine after ethanol feeding compared with mice on an isocaloric diet without ethanol (**Figure 2b; Supplemental Figure 2e, h**). Similarly, transcription of ERVs derived from gammaretroviral murine leukemia virus (MLV), including ecotropic MLV (*eMLV*), polytropic MLV (*pMLV*) and modified polytropic MLV (*mpMLV*), were significantly induced in the ileum of ethanol-fed microbiota humanized mice (**Supplemental Figure 2b**). Notably, ERVs were not induced by ethanol in the liver in any of the three models.

To determine whether increased ERV expression was detected by the host, we assayed the activation of Zbp1 and Mlkl-mediated necroptosis. Phosphorylated Mlkl assembles into oligomers, some of which translocate to the plasma membrane and induce necroptosis by causing rupture of the cell membrane (26). Intestinal epithelial cells isolated from ethanol-fed mice showed an increase in Zbp1 mRNA (**Figure 2c**) and protein expression, and increased Mlkl phosphorylation (**Figure 2d**). Hepatic *Zbp1* expression was not changed in mice subjected to the chronic-binge ethanol feeding (**Supplemental Figure 2c, f**), but it was induced in mice following intragastric hybrid feeding of ethanol (**Supplemental Figure 2i**) indicating that other factors besides ERVs can also stimulate Zbp1 expression. To extend these findings, we treated mouse intestinal organoids with different concentrations of ethanol (ranging from 10 to 50 mM) for 24 hours. Ethanol treatment led to a dose-dependent increase in *MMTV env* and *gag, eMLV, pMLV* and *mpMLV* expression (**Figure 2e; Supplemental Figure 3a**), *Zbp1* expression (**Figure 2f**), increased phosphorylation of Mlkl (**Figure 2g**), increased translocation from cytosol to membrane and oligomerization of Mlkl (**Figure 2h**), and increased cell death (**Figure 2i–j**). Ethanol did not increase apoptosis (cleaved caspase 3) or pyroptosis (cleaved gasdermin D) in intestinal organoids (**Supplemental Figure 3b**). These results might indicate that ethanol-induced ERVs signal through Zbp1 and Mlkl to induce necroptosis in intestinal epithelial cells.

Suppression of ERVs or inhibition of Mlkl reduces ethanol-induced necroptosis in intestinal organoids

We next treated intestinal organoids with the antiretrovirals emtricitabine or tenofovir for 24 hours and evaluated the effect on ethanol-induced necroptosis (**Figure 3a**). Treatment with emtricitabine or tenofovir led to a downregulation of ethanol-induced *MMTV env* and *gag* expression in intestinal organoids (**Figure 3b**), which was accompanied by reduced *Zbp1* expression (**Figure 3c**) and Mlkl phosphorylation (**Figure 3d**). In parallel, antiretroviral treatment resulted in a significant decrease in cytotoxicity following incubation with ethanol (**Figure 3e**). These results demonstrate that antiretroviral treatment reduces ethanol-induced ERV activation, activation of Zbp1/Mlkl signaling and cell death. Since antiretroviral treatment did not reduce cell death back to the level of control treated cells, we cannot rule out that other stimuli such as inflammatory cytokines or ethanol metabolites such as acetaldehyde might contribute to a lesser extent to ethanol-induced cell death.

To further understand the role of ethanol in inducting necroptotic death in intestinal epithelial cells, we investigated the effect of the Mlkl inhibitor GW806742X on ethanol-induced cell death (**Figure 3f**). Treatment of intestinal organoids with ethanol and GW806742X did not reduce ERV (*MMTV env* and *gag*) expression (**Figure 3g**) or *Zbp1* expression after 24 hours (**Figure 3h**). As expected, GW806742X blocked the ethanol-induced phosphorylation of Mlkl (**Figure 3i**). Importantly, treatment with GW806742X reduced ethanol-induced necroptosis in intestinal organoids (**Figure 3j**). We confirmed a decrease in ethanol-induced necroptosis following genetic knockdown of *Mlkl* in a mouse intestinal epithelial cell line, MODE-K cells (**Supplemental Figure 3c–d**). These results

222 indicate that ethanol triggers necroptosis by induction of ERV expression and activation
223 of the Mlkl signaling pathway in intestinal epithelial cells.
224
225 **Overexpression of HERV-K induces necroptosis in ethanol-treated intestinal cells**
226 To assess whether HERVs are able to directly induce necroptosis, we overexpressed
227 HERV-K in MODE-K cells in the presence or absence of ethanol (**Figure 4a–b**). HERV-
228 K overexpression significantly increased Zbp1 mRNA levels with and without ethanol
229 (**Figure 4c**). HERV-K overexpression also increased cell death, although only in presence
230 of ethanol, indicating that both HERV-K and ethanol are required for this effect (**Figure**
231 **4d**). Ethanol alone also triggered cell death, likely due to induction of mouse ERVs.
232 Importantly, the effect of HERV-K and ethanol in cell death was almost completely
233 attenuated by GW806742X, indicating that HERVK and ethanol induce necroptotic form
234 of cell death (**Figure 4d**).
235
236 **Antiretroviral treatment reduces ethanol-induced liver disease in microbiota**
237 **humanized mice**
238 To further investigate the role of ERVs in ethanol-induced liver disease *in vivo*, we
239 colonized germfree mice with stool from patients with alcohol-associated hepatitis (24).
240 Microbiota humanized mice were administered a combination of antiretrovirals
241 (emtricitabine, tenofovir, and nevirapine) (20) in a liquid diet and placed on a chronic-
242 binge ethanol or isocaloric diet as control, and ethanol-induced liver disease was studied
243 (**Figure 5a**). No significant differences were observed in body weight or food intake
244 (**Supplemental Figure 4a–b**). Antiretroviral treatment reduced *MMTV env* and *gag*

expression in the ileum and in intestinal epithelial cells isolated from the small intestine of ethanol-fed mice (**Figure 5b–c**). *MMTV env* and *gag* were not significantly induced in the liver following ethanol feeding (**Supplemental Figure 4c**). *Zbp1* gene expression was suppressed in the ileum and isolated intestinal epithelial cells from the small intestine of mice subjected to the chronic-binge ethanol feeding model and given antiretroviral treatment (**Figure 5d**). Furthermore, Zbp1 protein levels and Mlkl phosphorylation were significantly reduced in isolated small intestinal epithelial cells following ethanol feeding when treated with antiretrovirals (**Figure 5e–f**), indicating less necroptotic cell death in intestinal epithelial cells. Compared with vehicle treated mice, mice fed ethanol and receiving antiretrovirals developed less liver injury, indicated by a lower level of serum alanine amino-transferase (ALT) (**Figure 5g**), decreased hepatic steatosis (**Figure 5h–i**), and reduced liver inflammation with decreased expression of the inflammatory chemokines, chemokine (C-X-C motif) ligand-1 (*Cxcl1*) and *Cxcl2* (**Figure 5j**). Antiretrovirals also decreased the number of colony-forming units (CFU) of Gram-negative bacteria that translocated from the gut to the liver after ethanol feeding (**Figure 5k**). Using qPCR on genomic DNA isolated from liver tissue, we show a significant reduction in hepatic *E. coli* in ethanol-fed mice after antiretroviral treatment (**Figure 5l**). No significant differences were observed in serum level of ethanol or the mRNAs encoding the two primary enzymes that metabolize ethanol in the liver, alcohol dehydrogenase 1 (*Adh1*) and cytochrome P450 family 2 subfamily E polypeptide 1 (*Cyp2e1*) (**Supplemental Figure 4d–e**). Similarly, gene expression of *Cyp2e1* and *Adh1*, and of the acetaldehyde metabolizing enzyme aldehyde dehydrogenase 2 (*Aldh2*) was not significantly different in the duodenum between the different groups of ethanol-fed

mice (**Supplemental Figure 4f**). To compare the effect of antiretroviral treatment with a systemic Mlkl inhibitor, microbiota humanized mice were placed on a chronic-binge ethanol diet and treated with the Mlkl inhibitor GW806742X by intraperitoneal injection. Mice receiving GW806742X had significantly less liver injury and steatosis as compared with ethanol-fed mice. Antiretroviral treated mice had slightly, but significantly lower serum ALT levels as compared with GW806742X administered mice. Steatosis was similar between ethanol-fed mice receiving antiretrovirals or GW806742X (**Supplemental Figure 4g–h**).

These results indicate that antiretroviral therapy effectively attenuates ethanol-induced ERV activation, gut barrier dysfunction and liver disease.

Mice lacking *Zbp1* in intestinal epithelial cells are protected from ethanol-induced liver disease

To further corroborate the role of *Zbp1* in mediating the effect of ERVs in the intestine, we used mice with an intestinal epithelial cell (IEC)-specific deletion of *Zbp1* (*Zbp1*$^{\Delta IEC}$). This was achieved by generating a *Zbp1* conditional knockout mouse by CRISPR/Cas-mediated genome engineering, which was crossed to a villin-Cre transgenic mouse (**Supplemental Figure 5a**). qPCR and immunoblot analysis confirmed loss of Zbp1 expression in the intestine and intestinal epithelial cells, but not in the liver of *Zbp1*$^{\Delta IEC}$ mice as compared with *Zbp1*$^{fl/fl}$ littermates (**Supplemental Figure 5b–e**). Compared with *Zbp1*$^{fl/fl}$ mice, *Zbp1*$^{\Delta IEC}$ mice had less ethanol-induced liver injury (**Figure 6a**), steatosis (**Figure 6b–c**) and inflammation (**Figure 6d**) following chronic-binge ethanol feeding without change in body weight or food intake (**Supplemental Figure 5f–g**). Translocation

of viable *E. coli* to the liver was suppressed in ethanol-fed *Zbp1*$^{\Delta IEC}$ mice (**Figure 6e-f**). Absence of *Zbp1* in intestinal epithelial cells did not affect ERV expression in the intestine (**Figure 6g**) or the liver (**Supplemental Figure 5h**) following ethanol feeding. *Zbp1*$^{\Delta IEC}$ mice fed an ethanol diet showed less activation and phosphorylation of Mlkl in the intestine (**Figure 6h**). Intestinal absorption of ethanol, expression of hepatic and duodenal expression of genes involved in ethanol and acetaldehyde metabolism was similar in all groups (**Supplemental Figure 5i–k**).

To further support the importance of intestinal rather than hepatic Zbp1 in mediating the effect on ethanol-induced liver disease, we generated mice with specific deletions of *Zbp1* in Kupffer cells (*Zbp1*$^{\Delta KC}$) (**Supplemental Figure 6a–b**) and hepatocytes (*Zbp1*$^{\Delta Hep}$) (**Supplemental Figure 6h–i**). *Zbp1*$^{\Delta KC}$ or *Zbp1*$^{\Delta Hep}$ did not show significant differences in ethanol-induced liver disease compared with their respective *Zbp1*$^{fl/fl}$ littermates (**Supplemental Figure 6c–g, 6j–n**). Taken together, these findings demonstrate the critical role of intestinal epithelial Zbp1 in ethanol-induced liver disease.

Discussion

Our results provide new insights into the pathogenesis of alcohol-associated liver disease. We show that alcohol triggers ERV expression in the intestine, which leads to activation of Zbp1 and induction of the necroptosis pathway in intestinal epithelial cells. Consequently, the gut barrier becomes dysfunctional, allowing translocation of Gram-negative bacteria such as *E. coli* to the liver. Translocated bacteria in the liver are known to cause a progression of liver disease (27). And indeed, bacterial translocation and ethanol-induced liver disease are reduced by either suppression of ERVs using antiretrovirals or elimination of Zbp1 in intestinal epithelial cells (**Graphical Abstract**). Necroptosis is usually initiated in response to certain types of stress or infection, including viral infections (28). The necroptotic pathway controls infections by eliminating infected cells. In our study, ethanol exploits this pathway by inducing ERVs and stimulating innate immune responses, resulting in the elimination of intestinal epithelial cells and disruption of the gut barrier.

Our data show that HERV expression is induced in the intestine and the liver of patients with alcohol use disorder. In line with our results, mouse mammary tumor virus (MMTV-LV) env sequences (an ortholog of the human betaretrovirus) were found in 50% of liver samples from patients with alcohol-associated cirrhosis, but were not detected in normal liver (29). Consistent with the induction of hepatic HERVs in patients with alcohol-associated liver disease, ZBP1 protein expression is increased in the liver of patients with severe alcohol-associated hepatitis with a non-coding host-derived 5S rRNA pseudogene (RNA5SP) transcripts proposed as upstream activator (30). Ethanol causes epigenetic

changes and remodels the chromatin by histone modification such as acetylation (31, 32). It is possible that ethanol influences ERV expression through chromatin remodeling, but this requires further research.

Interestingly, ERVs are not induced in the liver of mice fed ethanol, while HERVs are elevated in the liver of patients with alcohol use disorder. Several factors could contribute to these differences. Mouse ERVs and HERVs are specific to their host genomes (33). Mechanisms for controlling the expression of these genetic elements might be different between mice and humans. Alcohol use disorder often leads to progressive liver disease in patients, while mice are resistant to developing advanced liver disease following ethanol administration. Therefore, the differential ERV response to ethanol between mice and humans might affect susceptibility to liver disease. Further research is required to delineate the role of HERV expression in the liver.

The antiretroviral drugs tenofovir and emtricitabine are nucleotide/nucleoside reverse transcriptase inhibitors and inhibit transcription of viral RNA into DNA. Since *MMTV env* and *gag* mRNA are suppressed after antiretroviral treatment and since tenofovir and emtricitabine do not inhibit transcription of reactivated ERVs, it is possible that there are replicative intermediates of exogenous retroviruses or active retrotransposition resulting in the formation of viral RNA/cDNA hybrids. And indeed, resurrection of endogenous retroviruses into infectious retroviruses has been described in immunodeficient mice (34). Nevirapine directly inhibits the reverse transcriptase enzyme and is specific for HIV, which is the reason it might have limited efficacy in our mouse model.

The precise mechanism linking necroptosis of intestinal epithelial cells to bacterial translocation remains unknown. Reactivation of ERVs in the intestine caused by dysfunctional *Setdb1*, induces Zbp1-mediated necroptosis, which triggers intestinal inflammation (21). Necroptosis might create gaps in the epithelial barrier, allowing bacteria to translocate into the underlying tissue and subsequently to the liver.

Taken together, we uncovered a process by which alcohol leads to viral mimicry by inducing ERVs in intestinal epithelial cells. This triggers Zbp1-mediated necroptosis in the intestinal epithelium and barrier disruption, causing bacterial translocation and progression of alcohol-associated liver disease.

Materials and methods

Sex as a biological variable

Male and female patients were used in this study. Male and female mice were used in this study.

Patient cohorts

Duodenal biopsies were obtained from 16 individuals without alcohol use disorder or alcohol-associated liver disease (controls), and 44 patients with alcohol use disorder and alcohol-associated liver disease at an alcohol withdrawal unit in Brussels, Belgium, where they underwent a detoxification and rehabilitation program. Demographic and laboratory characteristics of both controls and patients are detailed in **Supplementary Table 1**. Patients, who were actively drinking until the day of admission, underwent transient elastography with controlled attenuation parameter (CAP) (Fibroscan, Echosens, France) at admission. Upper endoscopy with biopsies was performed on day 2 after admission. Exclusion criteria included the use of antibiotics or immunosuppressive medication in the two months before enrollment, diabetes, inflammatory bowel disease, known liver disease of any other etiology, and clinically significant cardiovascular, pulmonary, or renal co-morbidities. Severity of liver disease was characterized using readily available clinical parameters. A median CAP value >250 dB/m was applied to diagnose steatosis (35), which was further confirmed by Doppler ultrasound. For distinguishing between non-progressive (simple steatosis) and progressive disease (steatohepatitis or steatofibrosis), criteria included ALT and AST levels >40 U/L, or a liver stiffness measurement (LSM) >

7.8 kPa (36). Specific thresholds for liver stiffness were utilized to differentiate between stages of fibrosis: an LSM of 7.6 kPa for F1/F2 and 8.8 kPa for F2/F3 (37).

Patients with suspected significant fibrosis ≥F2 on Fibroscan were routinely offered a transjugular liver biopsy. Initially, we used the cutoff of 7.8 kPa proposed by Nguyen-Khac et al. in 2008 (38). This cutoff was adapted to 9.0 kPa after publication of a meta-analysis by the same authors (39). Biopsy samples of ≥15 mm in length, including a minimum of 6 portal tracts, were considered suitable or when an experienced pathologist could establish the degree of fibrosis with certainty on a smaller sample. Twenty-seven patients consented to undergo a clinically indicated liver biopsy which was performed on the third day of admission. Demographic and biochemical data are summarized in **Supplementary Table 2**. Significant fibrosis (≥F2 according to the Metavir system) was confirmed on histology in 19 patients whereas 8 patients were down-graded to F1. Liver samples from size-reduced liver grafts were used as control. Histology revealed a normal appearance of the tissue. For ethical reasons and for protection of the donors' confidentiality, no additional data are available for those samples.

Mice

To assess ERV expression in mice, we employed three mouse models: 1) Germ-free female and male C57BL/6 mice (age 8 weeks) were bred in the gnotobiotic facility at UC San Diego as described (40). Germ-free status of the animals was routinely confirmed by plating fecal homogenates on blood agars and incubation for up to 2 days at 37°C under both aerobic (room air) and anaerobic (AnaeroPack System, Mitsubishi) conditions. Stool

from five different, HIV-negative patients with alcohol-associated hepatitis were used for fecal microbiota transplantation into germ-free mice. Mice were gavaged with 100 µL of stool samples (1 g stool dissolved in 30 ml Luria-Bertani (LB) medium containing 15% glycerol under anaerobic conditions), starting at an age of 4–5 weeks and repeated two weeks later. Two weeks after the second gavage, mice were placed on a chronic–binge ethanol diet (NIAAA model) or a control (isocaloric) diet as described (23). Mice were fed with a Lieber DeCarli diet, and the caloric intake from ethanol was 0% on days 1–5 and 36% from day 6 until the end of the study period. At day 16, mice were gavaged with a single dose of ethanol (5 g/kg body weight) in the early morning and euthanized 9 hours later. Pair-fed control mice received a diet with an isocaloric substitution of ethanol with dextrose. 2) Conventional male and female wild-type C57BL/6 mice were bred in our animal facility at the University of California San Diego, and placed on a chronic–binge ethanol diet (NIAAA model), or control (isocaloric) diet as described (23). 3) The hybrid model of intragastric chronic ethanol combines exposure of ethanol and western type high fat diet (25). This model was prepared by the Animal Core of the Southern California Research Center for ALPD and Cirrhosis. Briefly, C57BL/6 mice (age 8 weeks) were fed a solid western diet high in cholesterol and saturated fat (1% w/w cholesterol, 21% calories lard, 17% calories corn oil) for 2 weeks before surgery to implant an intragastric feeding catheter. After recovery, mice were fed a liquid high fat diet (36% calories corn oil) plus alcohol or isocaloric dextrose, plus weekly alcohol binge (3.5-5 g/kg) through the intragastric feeding tube. This intragastric feeding provided 60% of the required total daily caloric intake (614 calories/kg/day), and the remaining 40% of calories are consumed by

435 ad-lib consumption of solid western diet. The ethanol dose was increased to 27 g/kg/day
436 over 51 days. Pair-fed control mice were given an isocaloric high-fat liquid diet.
437
438 To assess the therapeutic efficacy of antiretroviral treatment, oral treatment with a
439 combination of emtricitabine (Cipla; 660 μM), tenofovir (Camber Pharmaceutical; 314 μM)
440 and nevirapine (Aurobindo; 375 μM) was given (20). Antiretrovirals were added to the
441 drinking water following the second fecal matter transplantation into germ-free mice from
442 four different, HIV-negative patients with alcohol-associated hepatitis. Antiretrovirals were
443 also included in the liquid diet at the start of the isocaloric feeding (day 0). Diets were
444 replaced every third day. Male and female mice were placed on a chronic–binge ethanol
445 diet (NIAAA model), or control (isocaloric) diet two weeks after the second gavage as
446 described above (23). A subset of mice was treated with the Mlkl inhibitor GW806742X
447 at a dose of 2 mg/kg by intraperitoneal injections three times a week while subjected to
448 the NIAAA model, using 10% dimethyl sulfoxide in saline as vehicle.
449
450 *Zbp1*-floxed mice were generated using CRISPR/Cas9 technology by Cyagen
451 Biosciences. Briefly, guide RNAs targeting the *Zbp1* gene were designed, and a donor
452 vector with loxP sites was co-injected with Cas9 mRNA into fertilized mouse eggs. Exons
453 2-3 were selected as conditional knockout regions. F0 founders were identified through
454 PCR and sequence analysis, and successful founders were bred with wild-type mice for
455 germline transmission. F1 animals were generated and confirmed by genotyping.
456 Molecular characterization verified the presence of the loxP-flanked *Zbp1* allele. Mice
457 lacking *Zbp1* in intestinal epithelial cells ($Zbp1^{\Delta IEC}$) were generated by crossing $Zbp1^{fl/fl}$

458 mice with intestinal epithelial cell-specific *villin*-Cre mice (41). Mice lacking *Zbp1* in Kupffer
459 cells (*Zbp1*$^{\Delta KC}$) were generated by crossing *Zbp1*$^{fl/fl}$ mice with Kupffer cell-specific *Clec4f-*
460 *Cre* mice (42). Mice lacking *Zbp1* in hepatocytes (*Zbp1*$^{\Delta Hep}$) were generated by crossing
461 *Zbp1*$^{fl/fl}$ mice with *albumin-Cre* mice (43). Female and male *Zbp1*$^{\Delta IEC}$, *Zbp1*$^{\Delta KC}$, *Zbp1*$^{\Delta Hep}$
462 and their respective control *Zbp1*$^{fl/fl}$ littermate mice (age, 8 weeks) were placed on a
463 chronic–binge ethanol diet (NIAAA model), or control (isocaloric) diet as described above
464 (23).
465
466 **Epithelial cell isolation**
467 The intestine was removed from mice, rinsed with cold PBS, opened longitudinally, and
468 cut into pieces of 1 cm length. Pieces were placed into ice-cold RPMI1640 medium
469 (Invitrogen) with 5% FCS containing DTT (1 mM). After vigorous shaking, the supernatant
470 was discarded, and the tissue was incubated for 20 min in RPMI1640 with 5% FCS
471 containing EDTA (1 mM) at 37 °C with shaking (250 rpm). Intestinal epithelial cells were
472 collected from supernatant.
473
474 **Overexpression of HERV-K**
475 The plasmids used for HERV-K overexpression have been described (44). In brief, a 785-
476 bp portion of *HERV-K* (corresponding to positions 7291–8076 in GenBank accession
477 number AF074086.2) was subcloned into a lentiviral shuttle vector (FUGW), downstream
478 of a nucleus-targeting GFP (NLS-GFP) reporter gene under the control of a strong
479 synthetic CAG promoter. Lentiviral particles were produced and packaged by Gene
480 Transfer, Targeting, and Therapeutics Core at the Salk Institute for Biological Studies, La

Jolla, CA. The following lentivirus constructs were used: BL-1161 (CAG-NLS-GFP-P2A, empty control vector) and BL-1177 (CAG-NLS-GFP-HML2(TLR), expressing the 785 nt HERV-K sequence). For HERV-K overexpression, lentiviral constructs were transduced into MODE-K cells using polybrene (Invitrogen). Infected MODE-K cells were selected with zeocin (Invitrogen) for 2 weeks and subsequently treated with 50 mM ethanol in the presence or absence of the Mlkl inhibitor GW806742X (2 μM; MedChemExpress) for 24hrs.

siRNA-mediated knockdown of Mlkl

MODE-K cells were transfected with specific small-interference RNA (siRNA) to silence the expression of Mlkl (siGENOME SMARTPool, M-005326-00-0005, Dharmacon) or non-targeting siRNA (siGENOME Non-Targeting siRNA Pool, D-001206-13-05, Dharmacon) for the control group. The transfection was performed using Lipofectamine 3000 Transfection Reagent (L3000008, Invitrogen) as follows: 0.1 nmol of each siRNA diluted in 300 μl of optiMEM (31985070, Life Technologies) was mixed with 15 μl of Lipofectamine 3000 diluted in 300 μl of optiMEM; the mixture was added into each well of 24 well plates; after 8 hours, the medium was replaced with fresh growth medium. 24 hours post transfection, cells were exposed to 100 mM ethanol. 48 hours post transfection, supernatant was collected for LDH measurement, and cells were collected to check the efficiency of silencing by quantitative PCR.

Human and mouse enteroids isolation and culture

Human colon biopsies were preserved in 500 µL medium (DMEM F-12 with 10% FBS, 200 mM Glutamax and penicillin/streptomycin) containing ROCK inhibitors (Y-27632, 10 µM and A-83-01, 10 µM) on ice and then immediately processed to generate intestinal organoids as described (45). Briefly, biopsies were washed with ice-cold DPBS (Gibco) and cut using two scalpels in a sterile petri dish. Tissues were incubated at 37°C with collagenase type I solution (2 mg/ml) for 30 min with intermittent shaking and then filtered through a 70 µm strainer into a 10-ml conical tube. Isolated crypts were embedded in 40 µL Matrigel (CLS356231-1EA, Corning/Sigma) in a 24-well plate and cultured in a modified form of medium.

Small intestinal organoids (enteroids) were generated from wild-type C57BL/6 as described (46). Briefly, crypts were collected from the mouse small intestine after 30 min incubation in PBS (pH 7.4) containing 2 mM EDTA at 4°C. Enteroids were plated in Matrigel (BD Bioscience) and maintained in DMEM/F12 (Life Technologies) containing ROCK inhibitors (Y-27632, 10 µM and A-83-01, 10 µM) and Fc–conditioned medium (the Rspo1-Fc–expressing cell line was a generous gift from Dr. Calvin Kuo, Stanford University, Stanford, CA). Cultures were passaged every 7–12 days and were typically split in a 1:6–1:8 ratio. To passage the three-dimensional human organoid cultures, organoids were treated with trypsin. Following centrifugation, the pellet was resuspended in Matrigel, plated at 40 µL per well in a 24-well plate, incubated at 37°C, 5% CO_2 for 10–20 minutes, and then 500 µL of conditioned medium was added to each well.

Intestinal organoids from mice or humans were treated with freshly prepared solutions of ethanol (Sigma, 54965) with concentrations ranging from 10 mM to 50 mM for 24 hours. GW806742X (2 μM; MedChemExpress) was added to organoid cultures for 24 hours to inhibit Mlkl. To assess the therapeutic efficacy of antiretroviral treatment, intestinal organoids were treated with emtricitabine or tenofovir disoproxil fumarate at a final concentration of 100 μM for 24 hours.

Primary mouse hepatocytes and Kupffer cells

Mouse hepatocytes were isolated from C57BL/6 mice as described (47). Hepatocyte viability was consistently >85% as determined by trypan blue staining (Thermo Fisher Scientific). Hepatocytes were collected directly after harvesting for further experiments. Kupffer cells were isolated as described (27). Briefly, Kupffer cells were isolated from the three-layer discontinuous density centrifugation gradient with 8.2% (wt/vol) and 14.5% (wt/vol) Nycodenz (Axis Shield). Kupffer cells were collected from the second layer. Cells were seeded into 6-well plates (1.5×10^6 cells per well) and incubated for two days. RPMI medium containing 10% FBS and antibiotics was used for Kupffer cells.

DNA extraction from mouse liver and feces

DNA was isolated from mouse livers as described (48). Briefly, samples were resuspended in PBS and digested with 20 μL RNAse A (100 mg/mL) and 10 μL proteinase K (20 mg/mL) at 55 °C for one hour. Each suspension was then transferred to individual Qbiogene lysing matrix B tubes and vortexed using a FastPrep FP120

instrument. The lysate was extracted twice using Phenol/Chloroform/Isoamyl alcohol, and DNA was precipitated, washed with ethanol, and resuspended in TE buffer.

Bacterial cultures of mouse liver

Translocation of viable bacteria was assessed by culturing liver homogenates (49). Liver tissues (~100 mg) were aseptically dissected, homogenized in 1 mL of 0.05% NP-40 solution, and incubated at 37°C for 3 hours. Post-incubation, samples were washed with PBS, centrifuged at 4,000 rpm for 10 minutes, and resuspended in 2 mL of PBS. For culture, 100 µL of the liver homogenate was plated on MacConkey agar plates and incubated overnight at 37°C under aerobic and anaerobic conditions. Colony counts were performed.

Biochemical analysis

Serum levels of alanine aminotransferase (ALT) were measured at 340 nm using ALT (SGPT) Kinetic (TECO Diagnostics). Hepatic triglyceride levels were measured using the Triglyceride Liquid Reagents Kit (Pointe Scientific). Levels of ethanol were measured using the Ethanol Assay Kit (BioVision). Cell cytotoxicity was assessed using Pierce LDH Cytotoxicity Detection Kit (Thermo Fisher Scientific).

Real-time quantitative PCR

RNA was extracted from liver and intestinal tissues using Trizol (Invitrogen). RNA was digested with DNase using the DNA-free DNA removal kit (Ambion), and cDNAs were generated using a high-capacity cDNA reverse transcription kit (Applied Biosystems).

Primer sequences for mouse genes were originally obtained from the NIH qPrimerDepot. All primers used in this study are listed in **Supplementary Table 3**. qPCRs for human and mouse gene expression, amplification of genomic bacterial DNA and single colonies were run with Sybr Green (Bio-Rad Laboratories) using an ABI StepOnePlus real-time PCR system. The expression levels of the gene of interest in mouse and human samples were normalized to the total amount of the housekeeping gene 18S. Additionally, bacterial PCR from liver samples was normalized using the 16S gene.

Oil Red O staining

To determine lipid accumulation, liver sections were embedded in OCT (Tissue-TekR) compound. 5 µm frozen sections were then cut and stained with Oil Red O (Sigma-Aldrich). Four representative microphotographs of each animal at 20X were taken with a BX51 Olympus microscope equipped with a DP72 Olympus digital camera, using Image J 2.9.0/1.53t software to quantify lipids (red area) from all Oil Red O-stained sections. Data were expressed as percentage of the control group.

Immunoblot analyses

Proteins were extracted and homogenized in 200 µl RIPA buffer (Thermo Scientific, San Diego, CA, USA) with phosphatase inhibitors (Sigma Aldrich, St. Louis, MO, USA) and protease inhibitors (Sigma Aldrich, St. Louis, MO, USA) as described (50). Total protein from intestinal organoids was extracted as described (51). For analysis of Mlkl in the subcellular compartments, the Subcellular Protein Fractionation Kit for Cultured Cells (ThermoScientific #78840) was used, subjecting whole organoid lysate to Cytoplasmic

Extractions Buffer and Membrane Extraction Buffer to obtain the cytoplasmic and membrane extracts, respectively. The proteins were resolved on polyacrylamide gels by SDS-PAGE (Biorad) under reducing or non-reducing conditions, and then transferred to polyvinylidene difluoride membranes (Bio-Rad Laboratories, Hercules, CA, USA). Immunoblot analysis was performed using anti-pMlkl antibody (1:1000) (Cell Signaling #37333), anti-Mlkl (1:1000) (Millipore #MABC604), anti-Zbp1 (1:1000) (Adipogen Life Science #AG-20B-0010-C100), anti-caspase 3 (1:1000) (Cell Signaling #9662), anti-cleaved caspase 3 (1:1000) (Cell Signaling #9664), anti-gasdermin D (cleaved and uncleaved) (1:1000) (ThermoFisher #MA5-44666), anti-Vdac (1:1000) (Cell Signaling #4866T) and anti-Gapdh (1:5000) (GeneTex #GT239/ GTX627408). Protein levels were normalized to Gapdh for each sample and expressed as arbitrary units (AU) in relation to the control group. Efficiency of fractionation was evaluated via Gapdh for cytoplasmic extracts and Vdac for membrane extracts. Densitometry was done using Image Lab 2.0 software (Bio-Rad Laboratories, Hercules, CA, USA). All uncropped immunoblots are shown in **Supplemental Figure 7**.

Statistical Analysis

Human data were expressed as median and interquartile range for each continuous outcome, if not stated otherwise. Continuous variables were compared using Mann-Whitney test. Categorical variables were compared using the Pearson's Chi-squared test. Spearman’s correlation was employed for correlation analysis. Results of the mouse studies are expressed as mean ± s.e.m. For mouse studies, significance between two groups were assessed by Mann-Whitney test, and significance between multiple groups

was assessed by One-way analysis of variance (ANOVA) with Tukey's post-hoc test or two-stage step-up method of Benjamini, Krieger and Yekutieli. A value of $p < 0.05$ was considered to be statistically significant. Statistical analyses were performed using R statistical software, R version 1.3.1093, 2020 the R Foundation for Statistical Computing and GraphPad Prism v8.4.3

Study approval

Written informed consent was obtained from all patients and controls, and the study protocol received approval from the Ethics Committee of the Université Catholique de Louvain in Brussels, Belgium. Colon biopsies were obtained from patients during a clinically indicated colonoscopy at the VA San Diego Healthcare System. Written informed consent was obtained from all subjects prior to the procedure. The study was approved by an institutional review board at the VA San Diego Healthcare System and at the University of California San Diego.

All animal studies were reviewed and approved by the Institutional Animal Care and Use Committees of the University of California San Diego and the University of Southern California, Los Angeles. Animal use adhered to the guidelines in the most recent edition of the Guide for the Care and Use of Laboratory Animals of the National Research Council of the United States National Academies and the Guidelines on Euthanasia by the American Veterinary Medical Association. Sample size estimation was based on previous studies, and animals were randomly allocated to experimental groups. No animals were excluded from the analysis.

Data availability

Raw data are listed in the accompanying excel file “Supporting data values”.

641 **Author contributions:** N.C. was responsible for the acquisition, analysis, and
642 interpretation of data, and writing the manuscript; M.F.F. was responsible for the
643 acquisition, analysis, and interpretation of data, and writing the manuscript; W.W., T.Y.,
644 F.R.T, A.E., A.S.M., S.M., and Y.W. provided assistance with data acquisition; R.G.C.
645 provided assistance with human and mice intestinal organoids; Y.M., L.E. and H.T.
646 provided assistance with conventional and gnotobiotic mouse studies; X.Z. provided
647 assistance with statistical analysis; D.E.F. and C.L. provided scientific advice and
648 technical support; T.T. and S.L. provided the lentiviral vector and technical support.; P.S
649 was responsible for collection of human samples; B.S. was responsible for the study
650 concept and design, study supervision and editing the manuscript. All authors reviewed
651 and edited the manuscript.
652
653 **Financial support:** M.F.F. is supported by the Galicia Regional Government & Fulbright
654 Fellowship (ED481B-2022-030) and an American Liver Foundation Postdoctoral
655 Research Fellowship Award. R.G.C. was supported by the AHA postdoctoral fellowship.
656 This study was supported in part by NIH grants R01 AA24726, R37 AA020703, U01
657 AA026939, P50 AA011999 (Project 1 and Animal Core) (B.S.); awards from the VA
658 Biomedical Laboratory Research & Development Service 1I01BX004594 (B.S.), 1I01
659 BX001991 (H.T.), and IK6BX004205 BLR&D Research Career Scientist Award (H.T.);
660 and services provided by NIH center P30 DK120515. P.S. received grant support from
661 Fond National de Recherche Scientifique Belgium (J.0146.17, T.0217.18 and T.0195.22)
662 and Action de Recherche Concertée (ARC 18/23-092), Université Catholique de Louvain,
663 Belgium.This study was supported in part by NIH grants R01 AA029106, R21 AA030654,

P30 AR073761 the D34 HP31027 UC San Diego's Hispanic Center of Excellence, by the American Association for the Study of Liver Diseases (AASLD) Pinnacle Research Award in Liver Disease (8998GA), and by the Isenberg Endowed Fellowship jointly awarded by the Pilot/Feasibility Program of the San Diego Digestive Diseases Research Center (SDDRC), the Hellman Family Foundation (P30 DK120515) (to C.L.).

Declaration of interests: B.S. has been consulting for Ferring Research Institute, HOST Therabiomics, Intercept Pharmaceuticals, Mabwell Therapeutics, Patara Pharmaceuticals, Surrozen and Takeda. B.S.’s institution UC San Diego has received research support from Axial Biotherapeutics, BiomX, ChromoLogic, CymaBay Therapeutics, NGM Biopharmaceuticals, Prodigy Biotech and Synlogic Operating Company. B.S. is founder of Nterica Bio. UC San Diego has filed several patents with B.S. as inventor.

References

1. Aberg F, Jiang ZG, Cortez-Pinto H, Mannisto V. Alcohol-associated liver disease-Global epidemiology. Hepatology. 2024.
2. Narro GEC, Diaz LA, Ortega EK, Garin MFB, Reyes EC, Delfin PSM, et al. Alcohol-related liver disease: A global perspective. Ann Hepatol. 2024:101499.
3. Hsu CL, Schnabl B. The gut-liver axis and gut microbiota in health and liver disease. Nat Rev Microbiol. 2023;21(11):719-33.
4. Fairfield B, Schnabl B. Gut dysbiosis as a driver in alcohol-induced liver injury. Jhep Rep. 2021;3(2):100220.
5. Wang L, Fouts DE, Starkel P, Hartmann P, Chen P, Llorente C, et al. Intestinal REG3 Lectins Protect against Alcoholic Steatohepatitis by Reducing Mucosa-Associated Microbiota and Preventing Bacterial Translocation. Cell Host Microbe. 2016;19(2):227-39.
6. Jiang L, Lang S, Duan Y, Zhang X, Gao B, Chopyk J, et al. Intestinal Virome in Patients With Alcoholic Hepatitis. Hepatology. 2020;72(6):2182-96.
7. Stoye JP. Studies of endogenous retroviruses reveal a continuing evolutionary saga. Nat Rev Microbiol. 2012;10(6):395-406.
8. Vargiu L, Rodriguez-Tome P, Sperber GO, Cadeddu M, Grandi N, Blikstad V, et al. Classification and characterization of human endogenous retroviruses; mosaic forms are common. Retrovirology. 2016;13:7.
9. Yi JM, Schuebel K, Kim HS. Molecular genetic analyses of human endogenous retroviral elements belonging to the HERV-P family in primates, human tissues, and cancer cells. Genomics. 2007;89(1):1-9.
10. Tristem M. Identification and characterization of novel human endogenous retrovirus families by phylogenetic screening of the human genome mapping project database. J Virol. 2000;74(8):3715-30.
11. Helmy M, Selvarajoo K. Systems Biology to Understand and Regulate Human Retroviral Proinflammatory Response. Front Immunol. 2021;12:736349.
12. Buttler CA, Chuong EB. Emerging roles for endogenous retroviruses in immune epigenetic regulation. Immunol Rev. 2022;305(1):165-78.
13. Chiappinelli KB, Strissel PL, Desrichard A, Li H, Henke C, Akman B, et al. Inhibiting DNA Methylation Causes an Interferon Response in Cancer via dsRNA Including Endogenous Retroviruses. Cell. 2015;162(5):974-86.
14. Stetson DB, Ko JS, Heidmann T, Medzhitov R. Trex1 prevents cell-intrinsic initiation of autoimmunity. Cell. 2008;134(4):587-98.
15. Tokuyama M, Kong Y, Song E, Jayewickreme T, Kang I, Iwasaki A. ERVmap analysis reveals genome-wide transcription of human endogenous retroviruses. Proc Natl Acad Sci U S A. 2018;115(50):12565-72.
16. Lima-Junior DS, Krishnamurthy SR, Bouladoux N, Collins N, Han SJ, Chen EY, et al. Endogenous retroviruses promote homeostatic and inflammatory responses to the microbiota. Cell. 2021;184(14):3794-811 e19.
17. Maelfait J, Liverpool L, Bridgeman A, Ragan KB, Upton JW, Rehwinkel J. Sensing of viral and endogenous RNA by ZBP1/DAI induces necroptosis. EMBO J. 2017;36(17):2529-43.

18. Zhang T, Yin C, Boyd DF, Quarato G, Ingram JP, Shubina M, et al. Influenza Virus Z-RNAs Induce ZBP1-Mediated Necroptosis. Cell. 2020;180(6):1115-29 e13.
19. Mocarski ES, Guo H, Kaiser WJ. Necroptosis: The Trojan horse in cell autonomous antiviral host defense. Virology. 2015;479-480:160-6.
20. Jiao H, Wachsmuth L, Kumari S, Schwarzer R, Lin J, Eren RO, et al. Z-nucleic-acid sensing triggers ZBP1-dependent necroptosis and inflammation. Nature. 2020;580(7803):391-5.
21. Wang R, Li H, Wu J, Cai ZY, Li B, Ni H, et al. Gut stem cell necroptosis by genome instability triggers bowel inflammation. Nature. 2020;580(7803):386-90.
22. Zhang G, Chen M, Graham D, Subsin B, McDougall C, Gilady S, et al. Mouse mammary tumor virus in anti-mitochondrial antibody producing mouse models. J Hepatol. 2011;55(4):876-84.
23. Bertola A, Mathews S, Ki SH, Wang H, Gao B. Mouse model of chronic and binge ethanol feeding (the NIAAA model). Nat Protoc. 2013;8(3):627-37.
24. Llopis M, Cassard AM, Wrzosek L, Boschat L, Bruneau A, Ferrere G, et al. Intestinal microbiota contributes to individual susceptibility to alcoholic liver disease. Gut. 2016;65(5):830-9.
25. Lazaro R, Wu R, Lee S, Zhu NL, Chen CL, French SW, et al. Osteopontin deficiency does not prevent but promotes alcoholic neutrophilic hepatitis in mice. Hepatology. 2015;61(1):129-40.
26. Ai Y, Meng Y, Yan B, Zhou Q, Wang X. The biochemical pathways of apoptotic, necroptotic, pyroptotic, and ferroptotic cell death. Mol Cell. 2024;84(1):170-9.
27. Duan Y, Chu H, Brandl K, Jiang L, Zeng S, Meshgin N, et al. CRIg on liver macrophages clears pathobionts and protects against alcoholic liver disease. Nat Commun. 2021;12(1):7172.
28. Koehler H, Cotsmire S, Zhang T, Balachandran S, Upton JW, Langland J, et al. Vaccinia virus E3 prevents sensing of Z-RNA to block ZBP1-dependent necroptosis. Cell Host Microbe. 2021;29(8):1266-76 e5.
29. Johal H, Scott GM, Jones R, Camaris C, Riordan S, Rawlinson WD. Mouse mammary tumour virus-like virus (MMTV-LV) is present within the liver in a wide range of hepatic disorders and unrelated to nuclear p53 expression or hepatocarcinogenesis. J Hepatol. 2009;50(3):548-54.
30. Wu J, Kim A, Wu X, Ray S, Allende DS, Welch N, et al. 5S rRNA pseudogene transcripts are associated with interferon production and inflammatory responses in alcohol-associated hepatitis. Hepatology. 2023;77(6):1983-97.
31. Kriss CL, Gregory-Lott E, Storey AJ, Tackett AJ, Wahls WP, Stevens SM, Jr. In Vivo Metabolic Tracing Demonstrates the Site-Specific Contribution of Hepatic Ethanol Metabolism to Histone Acetylation. Alcohol Clin Exp Res. 2018;42(10):1909-23.
32. Restrepo RJ, Lim RW, Korthuis RJ, Shukla SD. Binge alcohol alters PNPLA3 levels in liver through epigenetic mechanism involving histone H3 acetylation. Alcohol. 2017;60:77-82.
33. Chabukswar S, Grandi N, Lin LT, Tramontano E. Envelope Recombination: A Major Driver in Shaping Retroviral Diversification and Evolution within the Host Genome. Viruses. 2023;15(9).

34. Young GR, Eksmond U, Salcedo R, Alexopoulou L, Stoye JP, Kassiotis G. Resurrection of endogenous retroviruses in antibody-deficient mice. Nature. 2012;491(7426):774-8.
35. Karlas T, Petroff D, Sasso M, Fan JG, Mi YQ, de Ledinghen V, et al. Individual patient data meta-analysis of controlled attenuation parameter (CAP) technology for assessing steatosis. J Hepatol. 2017;66(5):1022-30.
36. Maccioni L, Gao B, Leclercq S, Pirlot B, Horsmans Y, De Timary P, et al. Intestinal permeability, microbial translocation, changes in duodenal and fecal microbiota, and their associations with alcoholic liver disease progression in humans. Gut Microbes. 2020;12(1):1782157.
37. Hsu C, Caussy C, Imajo K, Chen J, Singh S, Kaulback K, et al. Magnetic Resonance vs Transient Elastography Analysis of Patients With Nonalcoholic Fatty Liver Disease: A Systematic Review and Pooled Analysis of Individual Participants. Clin Gastroenterol Hepatol. 2019;17(4):630-7 e8.
38. Nguyen-Khac E, Chatelain D, Tramier B, Decrombecque C, Robert B, Joly JP, et al. Assessment of asymptomatic liver fibrosis in alcoholic patients using fibroscan: prospective comparison with seven non-invasive laboratory tests. Aliment Pharmacol Ther. 2008;28(10):1188-98.
39. Nguyen-Khac E, Thiele M, Voican C, Nahon P, Moreno C, Boursier J, et al. Non-invasive diagnosis of liver fibrosis in patients with alcohol-related liver disease by transient elastography: an individual patient data meta-analysis. Lancet Gastroenterol Hepatol. 2018;3(9):614-25.
40. Moody LV, Miyamoto Y, Ang J, Richter PJ, Eckmann L. Evaluation of Peroxides and Chlorine Oxides as Disinfectants for Chemical Sterilization of Gnotobiotic Rodent Isolators. J Am Assoc Lab Anim Sci. 2019;58(5):558-68.
41. Hartmann P, Haimerl M, Mazagova M, Brenner DA, Schnabl B. Toll-like receptor 2-mediated intestinal injury and enteric tumor necrosis factor receptor I contribute to liver fibrosis in mice. Gastroenterology. 2012;143(5):1330-40 e1.
42. Sakai M, Troutman TD, Seidman JS, Ouyang Z, Spann NJ, Abe Y, et al. Liver-Derived Signals Sequentially Reprogram Myeloid Enhancers to Initiate and Maintain Kupffer Cell Identity. Immunity. 2019;51(4):655-70 e8.
43. Bluemel S, Wang Y, Lee S, Schnabl B. Tumor necrosis factor alpha receptor 1 deficiency in hepatocytes does not protect from non-alcoholic steatohepatitis, but attenuates insulin resistance in mice. World J Gastroenterol. 2020;26(33):4933-44.
44. Dembny P, Newman AG, Singh M, Hinz M, Szczepek M, Kruger C, et al. Human endogenous retrovirus HERV-K(HML-2) RNA causes neurodegeneration through Toll-like receptors. JCI Insight. 2020;5(7).
45. Miyoshi H, Stappenbeck TS. In vitro expansion and genetic modification of gastrointestinal stem cells in spheroid culture. Nat Protoc. 2013;8(12):2471-82.
46. Sato T, Vries RG, Snippert HJ, van de Wetering M, Barker N, Stange DE, et al. Single Lgr5 stem cells build crypt-villus structures in vitro without a mesenchymal niche. Nature. 2009;459(7244):262-5.
47. Kouno T, Liu X, Zhao H, Kisseleva T, Cable EE, Schnabl B. Selective PPARdelta agonist seladelpar suppresses bile acid synthesis by reducing hepatocyte

CYP7A1 via the fibroblast growth factor 21 signaling pathway. J Biol Chem. 2022;298(7):102056.
48. Hsu CL, Wang Y, Duan Y, Chu H, Hartmann P, Llorente C, et al. Differences in Bacterial Translocation and Liver Injury in Ethanol Versus Diet-Induced Liver Disease. Dig Dis Sci. 2023;68(7):3059-69.
49. Phelps CM, Shapira JH, Laughlin CR, Meisel M. Detection of viable commensal bacteria in murine melanoma tumors by culturomics. STAR Protoc. 2023;4(3):102492.
50. Cabre N, Duan Y, Llorente C, Conrad M, Stern P, Yamashita D, et al. Colesevelam Reduces Ethanol-Induced Liver Steatosis in Humanized Gnotobiotic Mice. Cells. 2021;10(6).
51. Garcia-Carbonell R, Wong J, Kim JY, Close LA, Boland BS, Wong TL, et al. Elevated A20 promotes TNF-induced and RIPK1-dependent intestinal epithelial cell death. Proc Natl Acad Sci U S A. 2018;115(39):E9192-E200.

826 **Figure legends**

827 **Figure 1. Upregulation of Human Endogenous Retroviruses (HERVs) in duodenal**
828 **biopsies of patients with alcohol-associated liver disease**

829 **(a)** Duodenal biopsies were obtained from subjects without alcohol use disorder or
830 alcohol-associated liver disease (controls; n=16) and patients with alcohol use disorder
831 and alcohol-associated liver disease (n=44), and qPCR was performed to measure
832 mRNA expression of Human Endogenous Retroviruses (HERVs). **(b)** Duodenal
833 expression levels of HERVs in patients with advanced fibrosis (F2-F4) compared with
834 controls and patients with no or mild liver disease (F0-F1). **(c)** Liver biopsies were
835 obtained from subjects without alcohol use disorder or alcohol-associated liver disease
836 (controls, n=5) and patients with alcohol use disorder and alcohol-associated liver
837 disease (n=27) and qPCR was performed to measure mRNA expression of HERVs. **(d–**
838 **f)** Human intestinal organoids were treated with ethanol (50 mM) for 24 hours to assess
839 HERV expression **(e)** and to measure cytotoxicity using the lactate dehydrogenase (LDH)
840 assay of human organoids **(f)**. **(e–f)** Results were generated from 2 technical replicates.
841 P values among groups were determined by Mann-Whitney U test (**a, c, e–f**) or one-way
842 ANOVA with two-stage step-up method of Benjamini, Krieger and Yekutieli test (**b**).
843 Results are expressed as mean ± SEM. *P < 0.05, **P < 0.01, ****P < 0.0001.

844

845 **Figure 2**. **Ethanol activates Zbp1 and induces Mlkl-mediated necroptosis in**
846 **intestinal epithelial cells**

847 **(a)** Germ-free C57BL/6 mice were colonized with fecal microbiota from patients with
848 alcohol-associated hepatitis (AH) and fed oral isocaloric (control) or chronic–binge

ethanol diets. **(b)** Intestinal and hepatic levels of mouse mammary tumor virus (*MMTV*) *env* and *gag* mRNA. **(c)** Level of *Zbp1* mRNA in the ileum. **(d)** Intestinal epithelial cells were isolated from ethanol-fed mice, and immunoblots were performed for phospho-Mlkl, Mlkl, Zbp1, and Gapdh; protein amounts of Zbp1 relative to Gapdh, and protein amounts of phospho-Mlkl relative to Mlkl (n = 5 control, n=6 ethanol). **(e–j)** Mouse intestinal organoids were incubated with ethanol (0, 10, 20, and 50 mM) for 24 hours. **(e)** Expression levels of *MMTV env* and *gag* mRNA. **(f)** Expression level of *Zbp1* mRNA. **(g)** Immunoblots of phospho-Mlkl, Mlkl, and Gapdh; protein amounts of phospho-Mlkl relative to Mlkl (n = 5 in each group). **(h)** Immunoblot analysis of Mlkl in cytoplasmic and membrane extracts. Non-reducing and reducing SDS-PAGE were used to detect oligomerized and total Mlkl forms, respectively. **(i)** Representative images of intestinal organoids before and after treatment with ethanol (50 mM). **(j)** Lactate dehydrogenase (LDH) assay of supernatants was performed to measure cytotoxicity. Results were generated from three **(b)** or two **(c–j)** technical replicates. P values among groups were determined by Mann-Whitney U test **(b–d)** or one-way analysis of variance (ANOVA) with Tukey's post hoc test **(e–g, j)**. Results are expressed as mean ± SEM. AU, arbitrary units; FMT, fecal microbiota transplantation. *P < 0.05, **P < 0.01, ***P < 0.001, ****P < 0.0001.

Figure 3. Ethanol-induced necroptosis is reduced by suppressing ERV expression or inhibiting Mlkl in intestinal organoids

(a) Mouse intestinal organoids were treated with the antiretroviral agents emtricitabine (EC; 100 μM) or tenofovir disoproxil fumarate (TDF; 100 μM) and incubated with ethanol (50 mM) for 24 hours. **(b)** Expression levels of mouse mammary tumor virus (*MMTV*) *env*

and *gag* mRNA. **(c)** Expression level of *Zbp1* mRNA. **(d)** Immunoblots of phospho-Mlkl, Mlkl, and Gapdh; protein amounts of phospho-Mlkl relative to Mlkl (n = 4 in each group). **(e)** Lactate dehydrogenase (LDH) assay of supernatants was performed to measure cytotoxicity. **(f)** Mouse intestinal organoids were treated with the Mlkl inhibitor GW806742X (2 μM) and incubated with ethanol (50 mM) for 24 hours. **(g)** Expression levels of *MMTV env* and *gag* mRNA. **(h)** Expression level of *Zbp1* mRNA. **(i)** Immunoblots of phospho-Mlkl, Mlkl, and Gapdh; protein amounts of phospho-Mlkl relative to Mlkl (n = 5 in each group). **(j)** Lactate dehydrogenase (LDH) assay of supernatant was performed to measure cytotoxicity. Results were generated from three **(b–c)** or two **(d–j)** technical replicates. P values among groups were determined by one-way analysis of variance (ANOVA) with two-stage step-up method of Benjamini, Krieger and Yekutieli test **(b–e)** or Tukey's post hoc test **(g–j)**. Results are expressed as mean ± SEM. AU, arbitrary units; RTi, reverse transcriptase inhibitor. *P < 0.05, **P < 0.01, ***P < 0.001, ****P < 0.0001.

Figure 4. Overexpression of *HERV-K* induces necroptosis in ethanol-treated intestinal cells

(a) MODE-K cells were infected with a lentiviral control vector (Mock) or a lentivirus overexpressing Human Endogenous Retroviruses (*HERV*)-*K.* Infected MODE-K cells were treated with 50 mM ethanol and the Mlkl inhibitor GW806742X (2 μM) for 24 hrs. **(b)** Expression levels of *HERV-K* mRNA. **(c)** Expression level of *Zbp1* mRNA. **(d)** Lactate dehydrogenase (LDH) assay of supernatant was performed to measure cytotoxicity. **(b–d)** Results were generated from four technical replicates. P values among groups were

894 determined by one-way analysis of variance (ANOVA) with Tukey's post hoc test. Results
895 are expressed as mean ± SEM. *P < 0.05, **P < 0.01, ****P < 0.0001.
896
897 **Figure 5. Antiretroviral treatment reduces ethanol-induced intestinal necroptosis**
898 **and liver disease**
899 **(a)** Germ-free C57BL/6 mice were colonized with fecal microbiota from patients with
900 alcohol-associated hepatitis (AH) and treated with a combination of antiretrovirals
901 (emtricitabine 660 μM, tenofovir 314 μM, and nevirapine 375 μM) in the drinking water
902 after second colonization and then in liquid diet. Gnotobiotic mice were fed oral isocaloric
903 (control) or chronic–binge ethanol diets. **(b)** Levels of mouse mammary tumor virus
904 (*MMTV*) *env* and *gag* mRNA in the ileum. **(c)** Levels of *MMTV env* and *gag* mRNA in
905 intestinal epithelial cells (IECs) isolated from the small intestine. **(d)** Levels of *Zbp1* mRNA
906 in the ileum and in intestinal epithelial cells isolated from the small intestine. **(e–f)**
907 Intestinal epithelial cells were isolated from ethanol-fed mice and immunoblots were
908 performed for phospho-Mlkl, Mlkl, Zbp1, and Gapdh; protein amounts of Zbp1 relative to
909 Gapdh, and protein amounts of phospho-Mlkl relative to Mlkl (n = 8 in each group). **(g)**
910 Serum levels of ALT. **(h)** Hepatic triglyceride content. **(i)** Representative images of liver
911 sections stained with Oil Red O; scale bars, 200 μm. Quantification of Oil Red O-stained
912 area. **(j)** Hepatic levels of *Cxcl1* and *Cxcl2* mRNA. **(k)** Colony-forming units (CFU) on
913 MacConkey agar plates from the liver. **(l)** Hepatic *E. coli* abundance normalized to
914 bacterial 16S, as measured by qPCR. **(b–l)** Results were generated from two technical
915 replicates. P values among groups were determined by one-way analysis of variance
916 (ANOVA) with Tukey's post hoc test **(b, d left panel, g–i, l)** or Mann-Whitney U test **(c, d**

right panel, f, j–k). Results are expressed as mean ± SEM. AU, arbitrary units. *P < 0.05, **P < 0.01, ****P < 0.0001.

Figure 6. Deficiency of *Zbp1* in intestinal epithelial cells attenuates ethanol-induced intestinal necroptosis and liver disease

(a–h) Mice lacking *Zbp1* in intestinal epithelial cells (*Zbp1*$^{\Delta IEC}$) and their *Zbp1*$^{fl/fl}$ littermate controls were fed oral isocaloric (control) or chronic–binge ethanol diets. **(a)** Serum levels of ALT. **(b)** Hepatic triglyceride content. **(c)** Representative images of liver sections stained with Oil Red O; scale bars, 200 μm. Quantification of Oil Red O-stained area. **(d)** Hepatic levels of *Ccl2* and *Cxcl2* mRNA. **(e)** Colony-forming units (CFU) on MacConkey agar plates from the liver. **(f)** Hepatic *E. coli* abundance normalized to bacterial 16S, as measured by qPCR. **(g)** Levels of *MMTV env* and *gag* mRNA in the ileum. **(h)** Immunoblots of phospho-Mlkl, Mlkl, and Gapdh; protein amounts of phospho-Mlkl relative to Mlkl (n = 5 in each group). **(a–h)** Results were generated from two technical replicates. P values among groups were determined by one-way analysis of variance (ANOVA) with Tukey's post hoc test **(a–d, f–g)** or Mann-Whitney U test **(e, h)**. Results are expressed as mean ± SEM. AU, arbitrary units. *P < 0.05, **P < 0.01, ***P < 0.001, ****P < 0.0001.

Figure 1

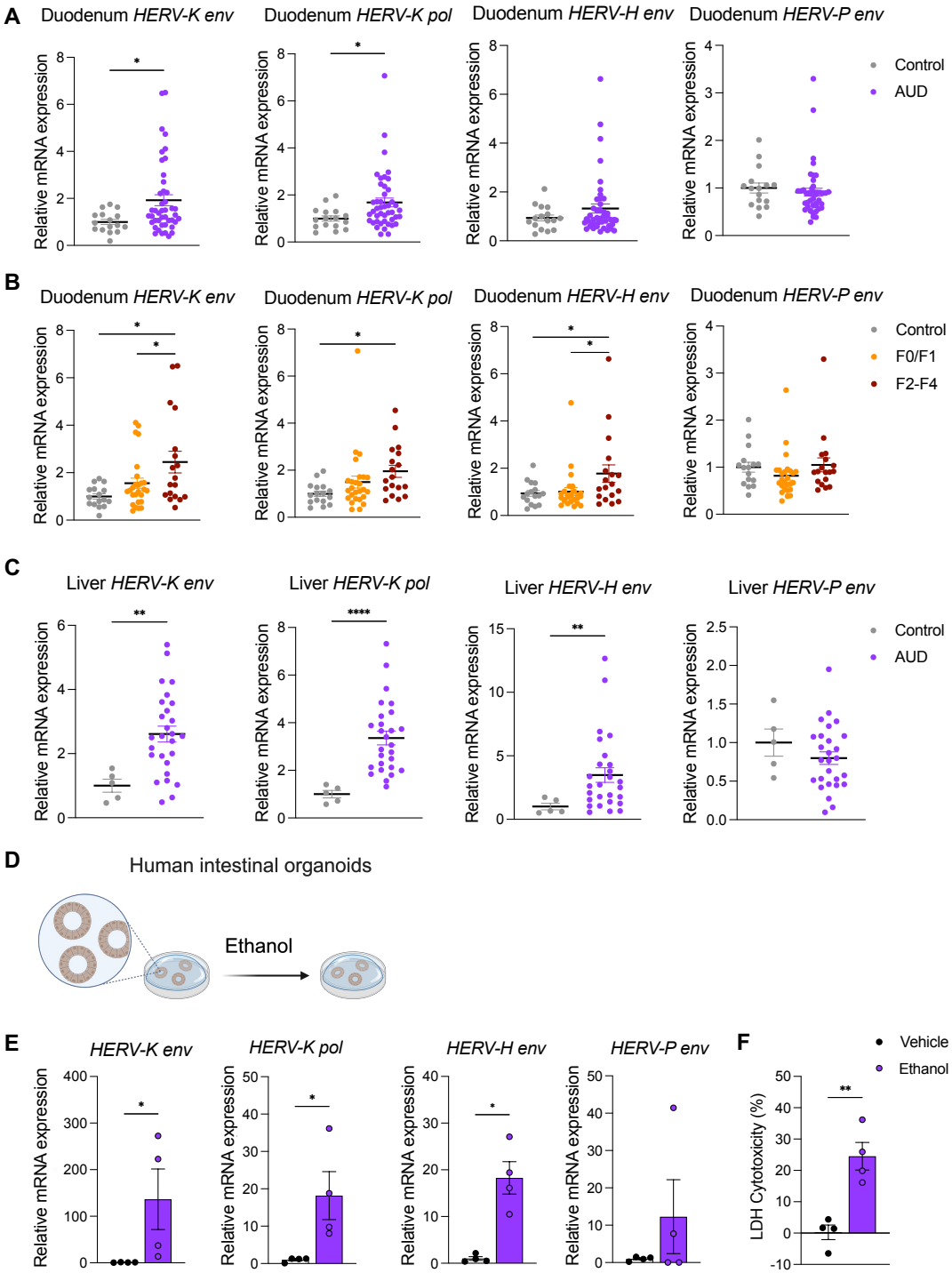
A
Duodenum HERV-K env
Duodenum HERV-K pol
Duodenum HERV-H env
Duodenum HERV-P env
Relative mRNA expression
Control
AUD
B
Duodenum HERV-K env
Duodenum HERV-K pol
Duodenum HERV-H env
Duodenum HERV-P env
Relative mRNA expression
Control
F0/F1
F2-F4
C
Liver HERV-K env
Liver HERV-K pol
Liver HERV-H env
Liver HERV-P env
Relative mRNA expression
Control
AUD
D
Human intestinal organoids
Ethanol
E
HERV-K env
HERV-K pol
HERV-H env
HERV-P env
Relative mRNA expression
F
Vehicle
Ethanol
LDH Cytotoxicity (%)

Figure 2

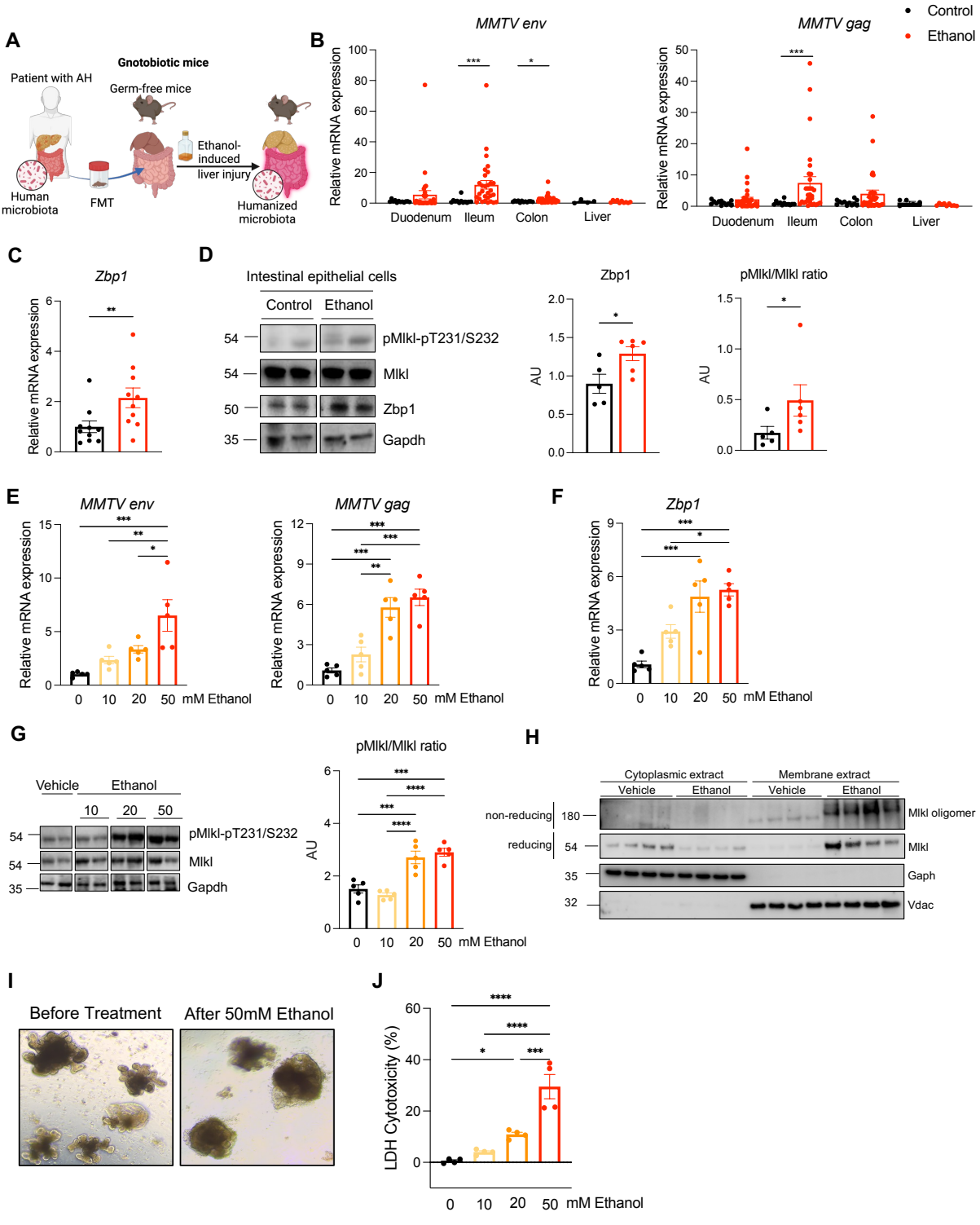
A
Gnotobiotic mice
Patient with AH
Germ-free mice
Ethanol-induced liver injury
Human microbiota
FMT
Humanized microbiota
B
MMTV env
MMTV gag
Control
Ethanol
Relative mRNA expression
Duodenum
Ileum
Colon
Liver
C
Zbp1
Relative mRNA expression
D
Intestinal epithelial cells
Control
Ethanol
pMlkl-pT231/S232
Mlkl
Zbp1
Gapdh
Zbp1
pMlkl/Mlkl ratio
AU
E
MMTV env
MMTV gag
Relative mRNA expression
0 10 20 50 mM Ethanol
F
Zbp1
Relative mRNA expression
0 10 20 50 mM Ethanol
G
Vehicle
Ethanol
10 20 50
pMlkl-pT231/S232
Mlkl
Gapdh
pMlkl/Mlkl ratio
AU
0 10 20 50 mM Ethanol
H
Cytoplasmic extract
Membrane extract
Vehicle
Ethanol
Vehicle
Ethanol
non-reducing
reducing
Mlkl oligomer
Mlkl
Gaph
Vdac
I
Before Treatment
After 50mM Ethanol
J
LDH Cytotoxicity (%)
0 10 20 50 mM Ethanol

Figure 3

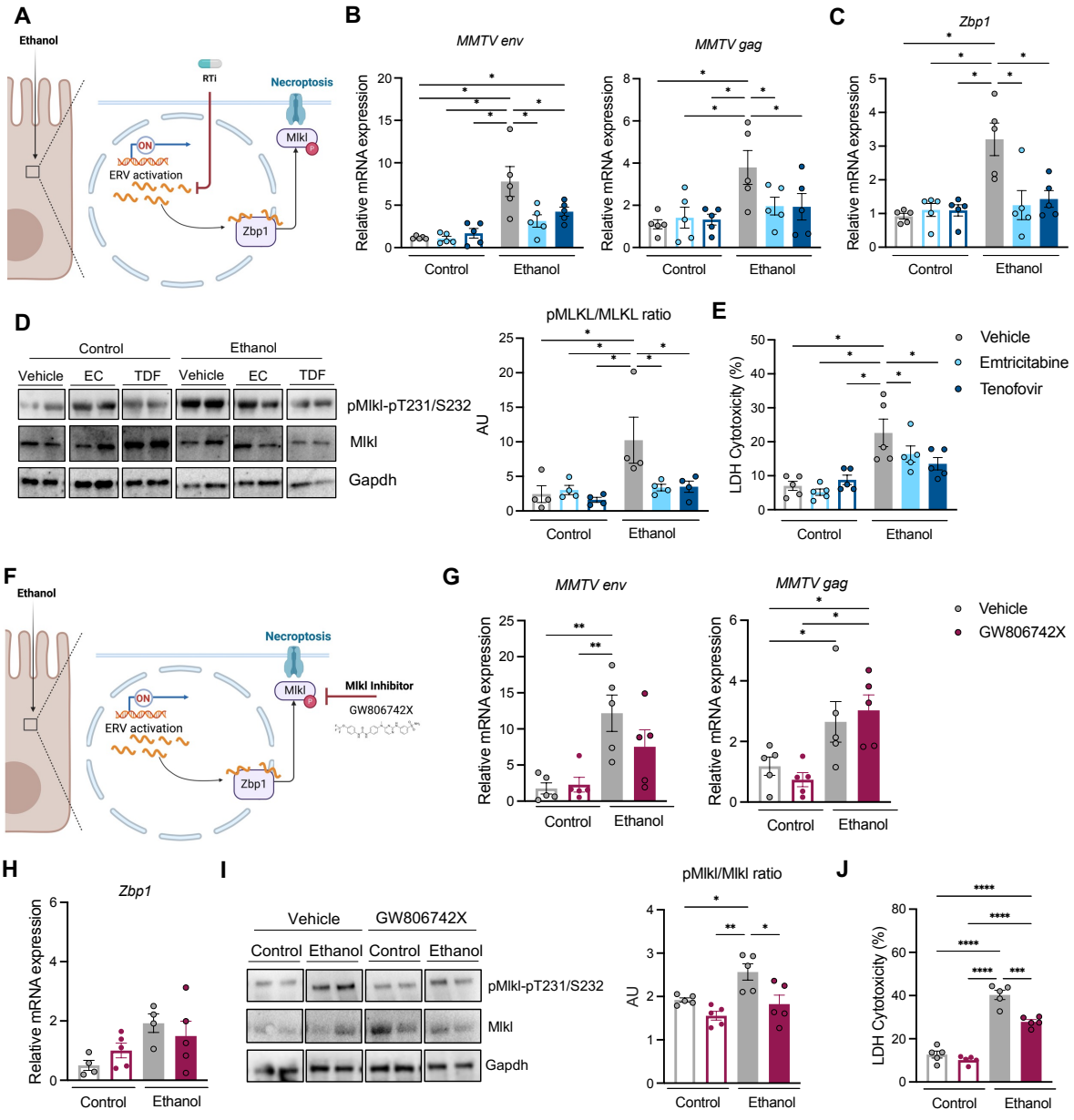
A
Ethanol
RTI
Necroptosis
Mlkl
ON
ERV activation
Zbp1
B
MMTV env
MMTV gag
Relative mRNA expression
Control
Ethanol
C
Zbp1
Relative mRNA expression
Control
Ethanol
D
Control
Ethanol
Vehicle
EC
TDF
Vehicle
EC
TDF
pMlkl-pT231/S232
Mlkl
Gapdh
pMLKL/MLKL ratio
AU
Control
Ethanol
E
LDH Cytotoxicity (%)
Control
Ethanol
Vehicle
Emtricitabine
Tenofovir
F
Ethanol
Necroptosis
Mlkl
Mlkl Inhibitor
GW806742X
ON
ERV activation
Zbp1
G
MMTV env
MMTV gag
Relative mRNA expression
Control
Ethanol
Vehicle
GW806742X
H
Zbp1
Relative mRNA expression
Control
Ethanol
I
Vehicle
GW806742X
Control
Ethanol
Control
Ethanol
pMlkl-pT231/S232
Mlkl
Gapdh
pMlkl/Mlkl ratio
AU
Control
Ethanol
J
LDH Cytotoxicity (%)
Control
Ethanol

936

Figure 4

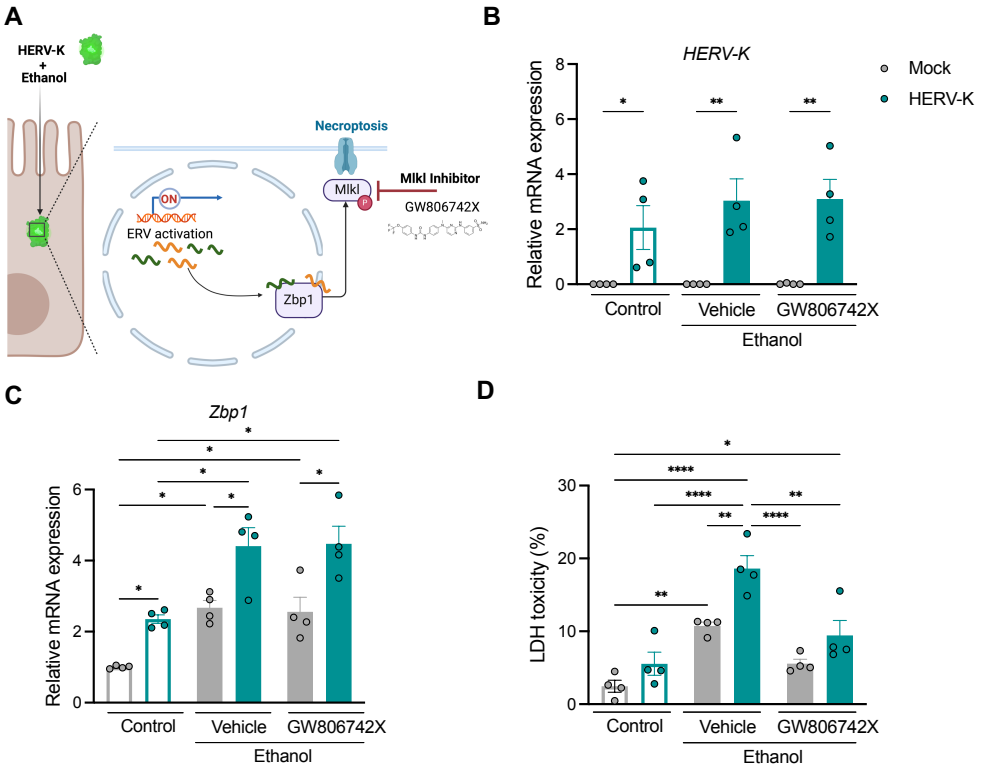
A
HERV-K
+
Ethanol
Necroptosis
Mlkl
Mlkl Inhibitor
GW806742X
ON
ERV activation
Zbp1
B
HERV-K
Mock
HERV-K
Relative mRNA expression
Control
Vehicle
GW806742X
Ethanol
C
Zbp1
Relative mRNA expression
Control
Vehicle
GW806742X
Ethanol
D
LDH toxicity (%)
Control
Vehicle
GW806742X
Ethanol

Figure 5

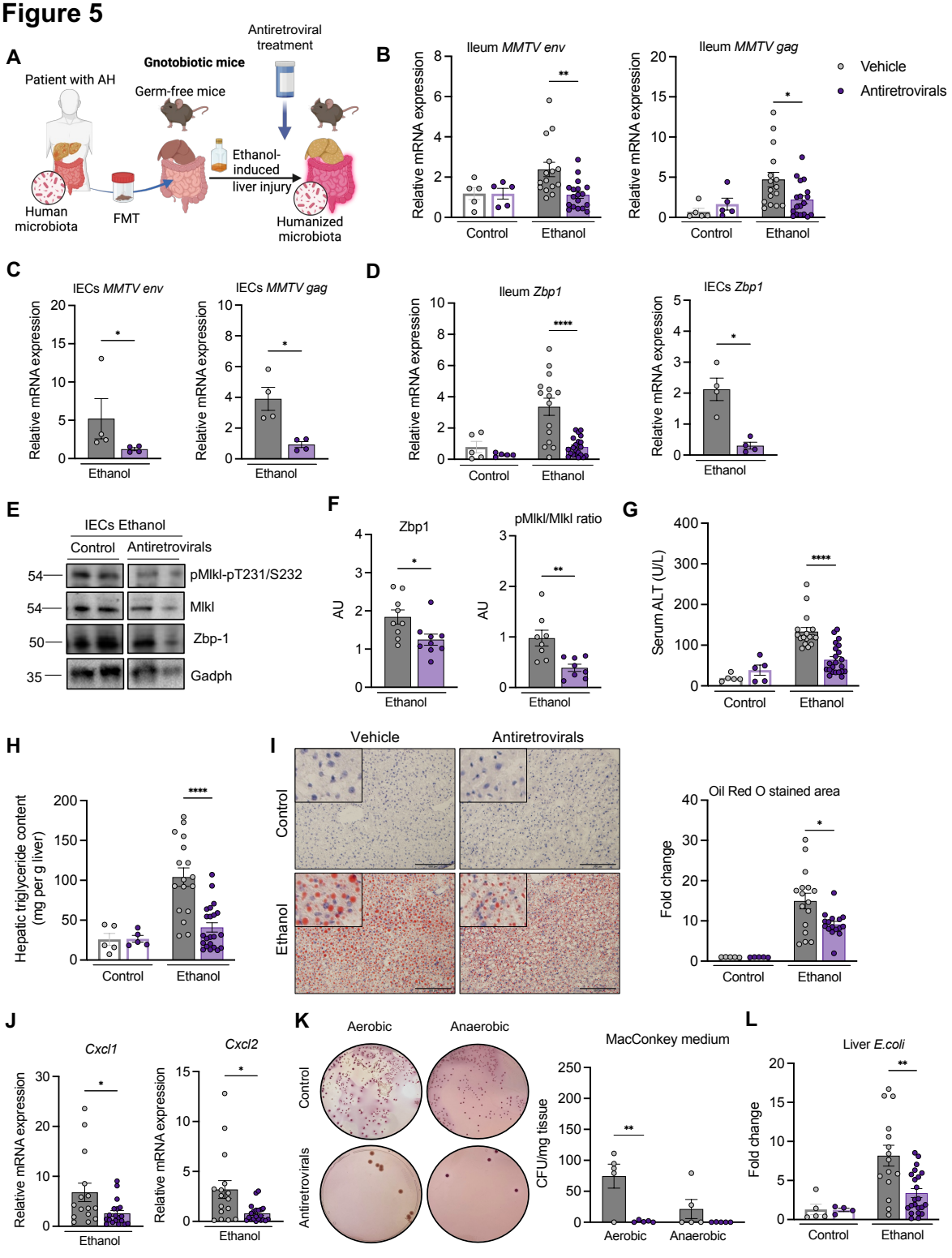
A
Patient with AH
Gnotobiotic mice
Germ-free mice
Antiretroviral treatment
Ethanol-induced liver injury
Human microbiota
FMT
Humanized microbiota
B
Ileum MMTV env
Ileum MMTV gag
Relative mRNA expression
Control
Ethanol
Vehicle
Antiretrovirals
C
IECs MMTV env
IECs MMTV gag
D
Ileum Zbp1
IECs Zbp1
E
IECs Ethanol
Control
Antiretrovirals
pMlkl-pT231/S232
Mlkl
Zbp-1
Gadph
F
Zbp1
pMlkl/Mlkl ratio
AU
G
Serum ALT (U/L)
H
Hepatic triglyceride content (mg per g liver)
I
Vehicle
Antiretrovirals
Oil Red O stained area
Fold change
J
Cxcl1
Cxcl2
K
Aerobic
Anaerobic
MacConkey medium
CFU/mg tissue
L
Liver E.coli

Figure 6

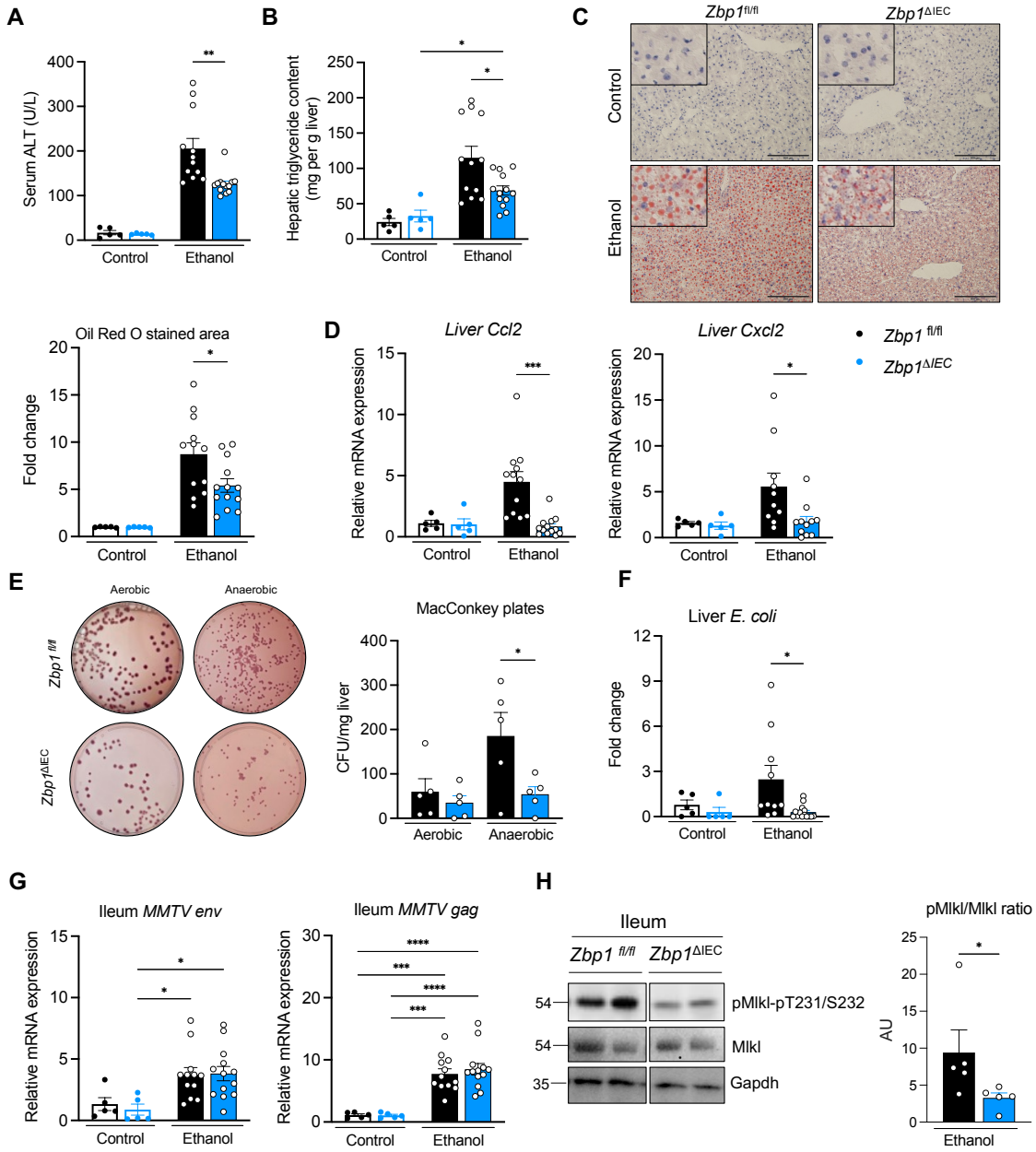
A
Serum ALT (U/L)
Control
Ethanol
B
Hepatic triglyceride content (mg per g liver)
C
Zbp1fl/fl
Zbp1ΔIEC
Control
Ethanol
Oil Red O stained area
Fold change
D
Liver Ccl2
Relative mRNA expression
Liver Cxcl2
Zbp1 fl/fl
Zbp1ΔIEC
E
Aerobic
Anaerobic
MacConkey plates
CFU/mg liver
F
Liver E. coli
Fold change
G
Ileum MMTV env
Ileum MMTV gag
Relative mRNA expression
H
Ileum
pMlkl-pT231/S232
Mlkl
Gapdh
pMlkl/Mlkl ratio
AU

939